JOC The Journal of Organic Chemistry

Article

pubs.acs.org/joc

Synthesis, Spectroscopic, and Analyte-Responsive Behavior of a Polymerizable Naphthalimide-Based Carboxylate Probe and Molecularly Imprinted Polymers Prepared Thereof

Ricarda Wagner,[†] Wei Wan,[‡] Mustafa Biyikal,[‡] Elena Benito-Peña,[§] María Cruz Moreno-Bondi,[§] Issam Lazraq,[†,#] Knut Rurack,*[,‡] and Börje Sellergren*[,†,⊥]

[†]Institute of Environmental Research (INFU), Faculty of Chemistry, Technical University of Dortmund, Otto-Hahn Strasse 6, D-44221 Dortmund, Germany

[‡]Division 1.9 Sensor Materials, BAM Federal Institute for Materials Research and Testing, Richard-Willstätter Strasse 11, D-12489 Berlin, Germany

[§]Chemical Optosensors & Applied Photochemistry Group (GSOLFA), Department of Analytical Chemistry, Faculty of Chemistry, Universidad Complutense de Madrid, E-28040 Madrid, Spain

[⊥]Department of Biomedical Sciences, Malmö University, SE-205 06 Malmö, Sweden

Supporting Information

ABSTRACT: A naphthalimide-based fluorescent indicator monomer **1** for the integration into chromo- and fluorogenic molecularly imprinted polymers (MIPs) was synthesized and characterized. The monomer was equipped with a urea binding site to respond to carboxylate-containing guests with absorption and fluorescence changes, namely a bathochromic shift in absorption and fluorescence quenching. Detailed spectroscopic analyses of the title compound and various models revealed the signaling mechanism. Titration studies employing benzoate and Z-L-phenylalanine (Z-L-Phe) suggest that indicator monomers such as the title compound undergo a mixture of deprotonation and complex formation in the presence of benzoate but yield hydrogen-bonded complexes, which are desirable for the molecular imprinting process, with weakly basic guests like Z-L-Phe. Compound **1** could be successfully employed in the synthesis of monolithic and thin-film MIPs against Z-L-Phe, Z-L-glutamic acid, and penicillin G. Chromatographic assessment of the selectivity features of the monoliths revealed enantioselective discrimination and clear imprinting effects. Immobilized on glass coverslips, the thin-film MIPs of **1** displayed a clear signaling behavior with a pronounced enantioselective fluorescence quenching dependence and a promising discrimination against cross-analytes.

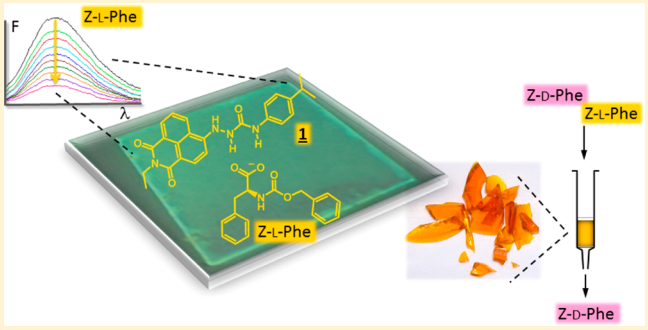

INTRODUCTION

Analyte-responsive polymers[1,2] in general and molecularly imprinted polymers (MIPs)[3,4] in particular are very promising materials in many areas of analytical chemistry. Particularly for purpose-fit sensing systems such as portable diagnostic devices, wearable sensors, or the chemically active components in microfluidic assemblies, tunable molecular recognition abilities and the format diversity of MIPs are very interesting and allow for tailored integration. However, for many such applications, it would be advantageous for MIPs to take a step from being a pure separation matrix to serving as an actual detection matrix, potentially reducing the detection protocol to a single step, continuous and direct. Such advancements require the integration of a signaling element into the imprinted polymer. Because many sensor formats as alluded to above operate with light as the interrogating medium, a promising approach is the integration of chromo- and/or fluorogenic indicator molecules directly into the MIP. These molecular indicators should undergo a change in either absorption and/or preferably fluorescence upon rebinding of the analyte in the MIP. Although several studies on using conventional MIPs for the detection of fluorescently tagged analytes,[5,6] which again is at least a two-step process, on employing MIPs with simple fluorophores embedded for the detection of quenchers[7,8] or on competitive assays involving fluorescently labeled imprints[9,10] have been published in the past, few examples of the integration of a polymerizable chromo- and/or fluorogenic probe have been reported until now. In particular, examples that show directional recognition at a designated binding site[11,12] or responses in the analytically advantageous visible spectral range are scarce.[12−14]

Received: September 8, 2012
Published: January 28, 2013

In our present work, we chose the 4-amino-substituted naphthalimide (NI) chromophore as the scaffold because such dyes usually emit strong fluorescence in the analytically advantageous region >500 nm and can be excited in the near visible at ca. 420−450 nm,[15,16] a range for which low-cost excitation sources are readily available. In addition, the NI unit is a popular building block in fluorescent probes for various analytes,[17,18] can be integrated into polymers,[19,20] and has also been successfully employed in anion-responsive probes.[21,22] On the basis that many of the key targets as templates/analytes in our MIP research carry at least one carboxylic acid group,[23,24] the latter features are very interesting and motivated us to pursue the synthesis of the polymerizable NI-based anion probe **1** (Chart 1). Here, we report on the synthesis, spectroscopic, and analyte-responsive behavior of **1** and its integration into monolithic and thin-film MIPs for a first assessment of the separation and sensing performance of such intrinsically fluorogenic molecularly imprinted polymers.

Chart 1. Chemical Structure of Title Monomer 1

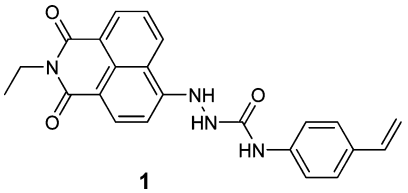

1

RESULTS AND DISCUSSION

The synthesis of the urea-based monomer **1** follows the path illustrated in Scheme 1. Starting from commercially available 4-bromo-1,8-naphthalic anhydride, **1** is obtained in three steps in an overall acceptable yield. Because initial attempts to reproduce the syntheses of **3** published in refs 25 and 26 failed, we modified this step of the reaction sequence. The successful synthesis of **1**−**3** was proven by NMR and MS spectroscopic methods (Figure 1A). As a polymerizable probe monomer, **1** is composed of three functional units. The *N*-ethyl-4-amino-1,8-naphthalimide fragment presents the actual chromophoric entity. The directly electronically fused urea group is responsible for the binding of the analyte. The direct conjugation between both units should guarantee an efficient transduction of the binding event into a spectroscopic signal. The styrene moiety, again fused directly to the urea unit, has two roles. On one hand, it contains the reactive linker for the copolymerization into the MIP matrix. On the other hand, aryl substitution at the urea commonly increases the receptor's affinity toward anionic guests because the attachment of an aryl moiety leads to a higher acidity of the respective NH group.[27]

Scheme 1. Schematic Representation of the Synthesis of 1

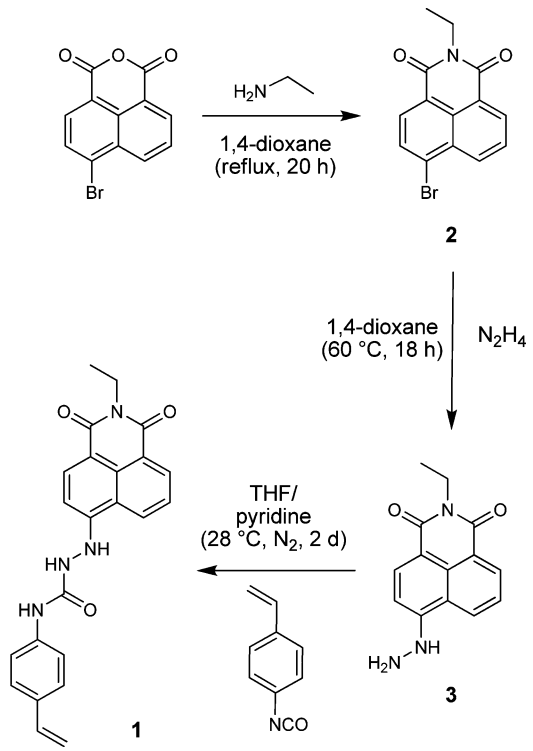

To assess whether the probe under consideration is suitable for the molecular imprinting process and whether it supposedly performs in the desired analytical fashion, the following requirements should be met. For the first task it is important that the complex between fluorescent monomer and template is stable under conventional imprinting conditions. This is commonly the case when the complex stability constant lies on the order of K = 1000 M^{-1} or higher in polar organic solvents such as acetonitrile or DMSO. The second requirement concerns the spectroscopic behavior of the probe monomer as such and in the presence of the analyte in the respective solvents mentioned previously.

Spectroscopic Properties of 1. Representative absorption and fluorescence spectra of **1** are shown in Figure 1B. It is apparent that the typical features of 4-aminonapthalimide chromophores are retained in **1**, i.e., a broad and nonstructured absorption band with a maximum at ca. 400 nm and a strongly Stokes shifted, broad emission band at ca. 500 nm (for detailed data, see Table 1), in contrast to the structured and blue-shifted bands of 1,8-naphthalimides lacking an amino group in the 4-position such as **4** and **5** with λ_{abs} ca. 345 and λ_{em} ca. 375 nm[28,29] (for chemical structures, see Chart 2). Moreover, detailed spectroscopic studies of **1** as a function of solvent polarity revealed a positive solvatochromism, i.e., absorption and emission bands gradually shift to longer wavelength with increasing polarity of the solvent (Table 1). In accordance with established NI photophysics,[15] these properties hint at an intramolecular charge transfer (ICT) process being active in **1**. For comparison, **6** (Chart 2) shows absorption and fluorescence maxima of 413 and 513 nm in acetonitrile and 420 and 500 nm in THF.[15] Alkyl substitution shifts these values slightly to 415 and 528 nm (MeCN) and 408 and 508 nm (THF) for **7** (Chart 2) due to the higher donor strength of the dimethylamino compared with the amino group.[15] The attached urea-styryl moiety thus has only a minor influence on the ICT process in the NI chromophore. (Note that the different nature of the alkyl substituents at the imide nitrogen, *n*-butyl in ref 15 and ethyl in our case, has virtually no influence on the photophysics.[29])

With regard to fluorescence quantum yields and lifetimes, the substitution pattern at the 4-amino nitrogen atom, however, is a more decisive factor. Going back to **4** and **5** with electronically rather weakly interacting substituents at the 4-position, these NI dyes display largely quenched fluorescence because of efficient coupling of energetically close-lying nπ^* states.[28,29] In contrast, when a primary or secondary amino group is in the 4-position like in **6** and **8**, high fluorescence quantum yields

dx.doi.org/10.1021/jo3019522 | J. Org. Chem. 2013, 78, 1377−1389

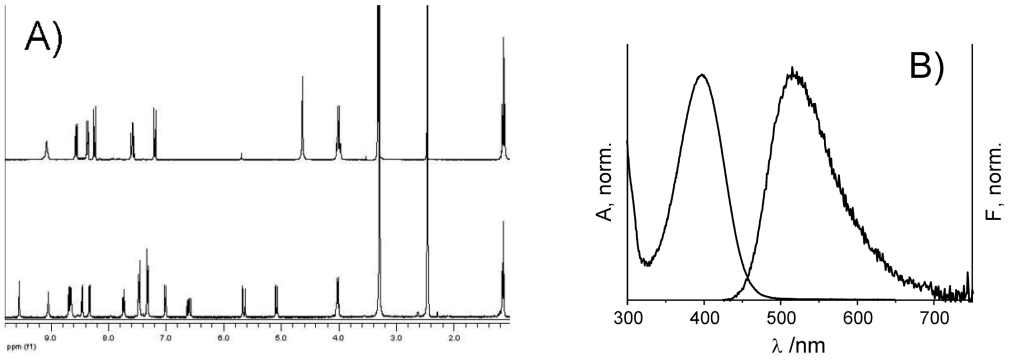

Figure 1. (A) NMR spectra of **1** (bottom) and **3** (top) in DMSO. (B) Absorption and fluorescence spectra of **1** in acetonitrile at 298 K.

Table 1. Spectroscopic Properties of 1 and 3 in Selected Solvents

compd	solvent	λ_{abs} /nm	λ_{em} /nm	Φ_f	τ_f /ns
1	DMSO	420	542	0.018	0.11
1	EtOH	412	535	0.013	0.07
1	MeCN	404	517	0.015	0.12
1	THF	402	512	0.020	0.13
1	dioxane	392	500	0.040	0.46
3	MeCN	425	516	0.008	0.01

Chart 2. Chemical Structures of Model Compounds Discussed in the Text (Me = Methyl, Et = Ethyl, nPr = *n*-Propyl, nBu = *n*-Butyl)

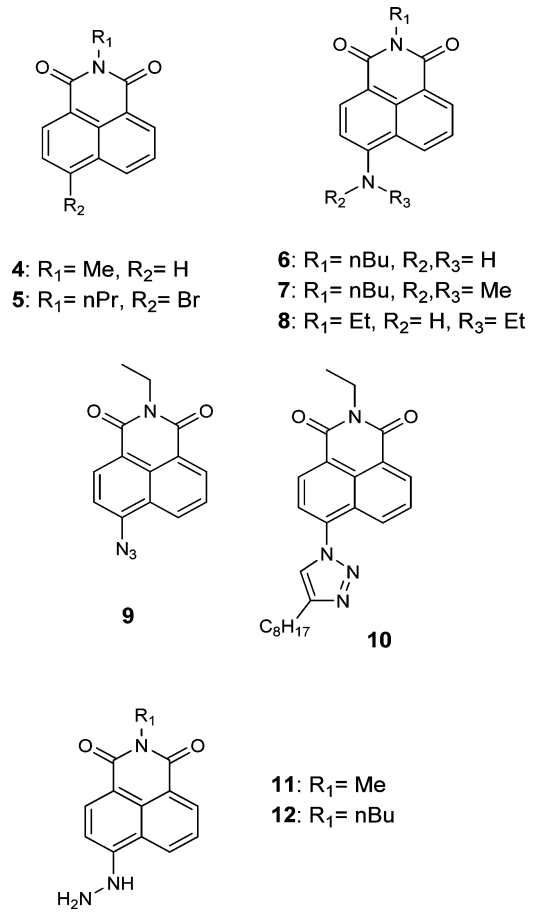

emerge (e.g., ≥0.6 in ethanol[15,29]), yet with a tertiary amine like in **7**, Φ_f is again considerably lower (e.g., 0.01 in ethanol[15]). Saha and Samanta attributed this behavior to the formation of a highly emissive ICT state in **6** and **8** which is quenched in **7** because of accelerated inversion at the nitrogen center in the 4-position and/or the influence of a close-lying dark state.[15] If we now consider **3**, the fluorescence is also quenched although the molecule should be more reminiscent of **6**. Since **3** is planar and entirely π-conjugated, photoinduced electron-transfer-type quenching can be ruled out as an active process. Moreover, because the spectroscopically important transitions are distinctly lower in energy as for **4** and **5**, nπ^* state interaction is also unlikely. However, if we also take into account the behavior of other NI derivatives with highly electron-rich nitrogen-containing substituents at the 4-position, i.e., virtually no fluorescence in the case of **9**[30] and a moderate fluorescence of Φ_f = 0.21 in MeCN in the case of **10** (for chemical structures, see Chart 2), which are all π-conjugated and not particularly sterically hindered, the quenching process should be related to intrinsic electronic properties of the molecules. Indeed, quantum chemical calculations performed on **1**, **3**, and **6**–**10** revealed that the order of emissivity seen in these dyes (**9** < **3** ∼ **1** ∼ **7** < **10** < **8** < **6**) basically corresponds to the singlet–triplet energy gap for the lowest and second lowest excited states and hence the probability of accelerated nonradiative deactivation via intersystem crossing.[31] (Note: Recently, Φ_f = 0.65 and 0.51 in acetonitrile, which are almost 2 orders of magnitude higher than Φ_f of **3** determined by us here, have been reported for **11** and **12** (Chart 2), i.e., for closely related analogues of **3** varying only in the spectroscopically silent alkyl substituent at the imide nitrogen atom.[26] Because we were not able to synthesize **3** under the conditions employed by those authors and all our other experimental and theoretical considerations do not support such high fluorescence for this type of molecule, we tentatively assume that the earlier reported values are erroneous.)

Spectrophotometric Response of 1 toward Carboxylates. Having established the underlying photophysical processes in **1**, we investigated the response of the functional monomer toward oxyanionic guest molecules by different types of experiments and employing tetrabutylammonium benzoate (TBAB) and Z-L-phenylalanine (Z-L-Phe) as model templates. To assess the ground-state interaction of **1** and benzoate (Bz^-), spectrophotometric titrations were performed in THF, MeCN, and DMSO. Figure 2 shows the color changes in DMSO visible to the naked eye, with the color developing from bright yellow through dark yellow and green to brownish-orange upon addition of increasing amounts of TBAB up to 10 equiv.

Upon closer inspection of the guest-induced spectroscopic changes by spectrophotometric measurements as shown in

dx.doi.org/10.1021/jo3019522 | J. Org. Chem. 2013, 78, 1377–1389

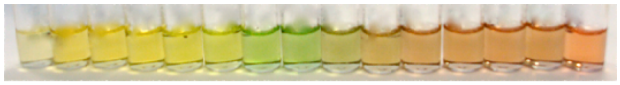

Figure 2. Visible color changes induced by Bz^- addition to a solution of **1** in DMSO.

Figure 3, it is apparent that the addition of the anionic guest leads to a pronounced decrease of the typical NI absorption band at 420 nm in DMSO with a concomitant development of a new broad band with a global maximum at ca. 570 nm (Figure 3A). Similar features though less pronounced are found in MeCN (Figure 3B). On the other hand, the behavior in THF is different. Again, a strongly red-shifted broad band appears as a shoulder at ca. 530−570 nm. However, in this solvent the main ICT absorption band of **1** is shifted from 402 to 434 nm (Figure 3C). Dramatic bathochromic shifts of >100 nm as seen here point to a significant electronic modulation of an ICT chromophore which is usually not obtained by simple coordination of an anionic species through two hydrogen bonds, the anticipated binding mode between ureas and carboxylates, especially since the urea moiety is not directly fused to the NI core (Scheme 2, route A).[32] The behavior in DMSO thus suggests that the secondary 4-amino group in **1** is rather acidic and is gradually deprotonated with no apparent hints of the formation of a hydrogen bonded complex with benzoate, presumably also because the solvent can successfully compete (Scheme 2, route B). Similar deprotonation-induced red-shifts have also been found for other NI derivatives substituted with extended functional groups at a secondary 4-amino nitrogen.[33] In contrast, in less strongly coordinating solvents such as MeCN or THF, TBAB is still basic enough to deprotonate **1** yet the lack of the solvent to interact with the urea group might lead to the formation of two different species. One possibility is an equilibrium between the intramolecularly stabilized and the nonstabilized species in Scheme 2, route C. (Note that according to quantum chemical calculations the two anionic structures on the product side of route C are the most stable structures of the various anion isomers/tautomers that are theoretically possible because of the three NH groups and respective tautomeric equilibria in the hydrazinecarboxamide system.[31]) The other possibility is that at higher excess, Bz^- coordinates to the urea group in the designated fashion (Scheme 2, route A).

Further insight into the possible mechanisms at play can be obtained from an analysis of the association constants K extracted from the different titrations. These data, derived by nonlinear regression fitting, are collected in Table 2. As would be expected, the association constant strongly depends on the solvent used. The affinity of the host monomer toward the oxyanionic guest is most pronounced in the least competitive solvent, namely THF. However, it is also surprising that analysis of the titration data at different spectral positions yields different results in the case of MeCN and especially THF. This discrepancy, which is reflected by the fact that the isosbestic points in MeCN and particularly THF are not as sharp as in DMSO, suggests that more than two species are involved in the processes happening during the titration. Accordingly, we subjected the titration spectra to a nonlinear fitting process to extract the equilibrium constants for deprotonation and/or hydrogen bonding complex formation. In the case of DMSO, a 1:1 de- or reprotonation model with the global equilibrium MH + B^- ⇌ M^- + BH (with MH equaling **1**, M^- = $\mathbf{1}^-$, B^- = Bz^-; the TBA counterion was not taken into account) yielded an acceptable fit and a log K = 3.93 ± 0.01.[34] This value is in good

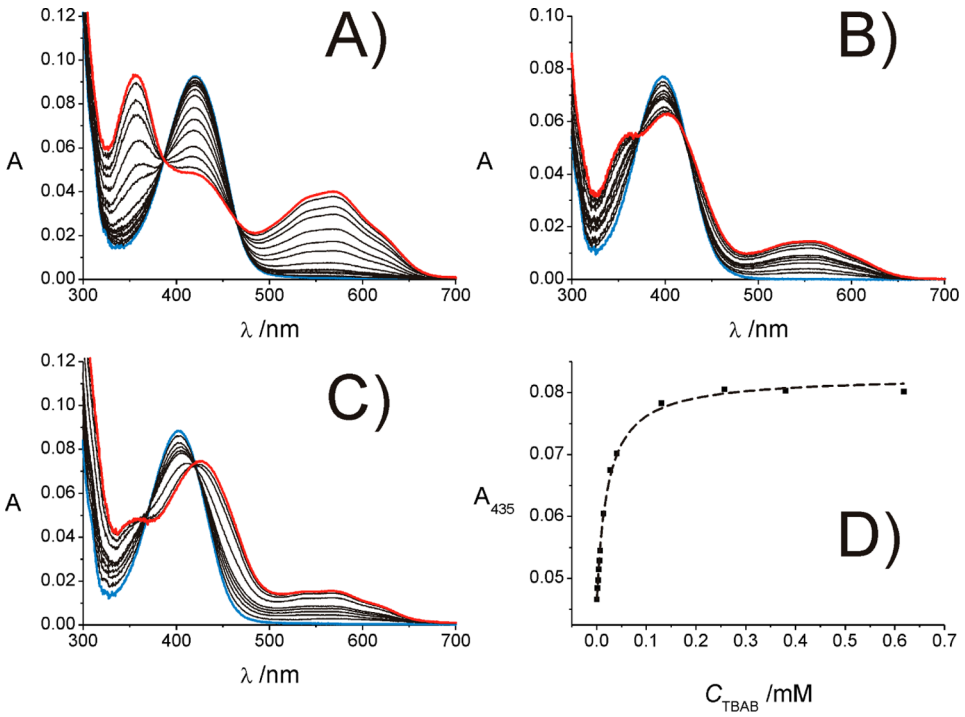

Figure 3. Absorption titration spectra of **1** and TBAB in DMSO (A), acetonitrile (B), and THF (C) (starting point spectra in blue, end point spectra in red) and representative titration curve (fit as dashed line) obtained from a plot of A_{435} vs c_{TBAB} in THF (D); c_1 = 7 μM, c_{TBAB} = 1.5−600 μM (different step sizes).

dx.doi.org/10.1021/jo3019522 | J. Org. Chem. 2013, 78, 1377−1389

Scheme 2. Possible Hydrogen Bonding and Deprotonation Pathways Involving 1, Benzoate, and Specific Solvents

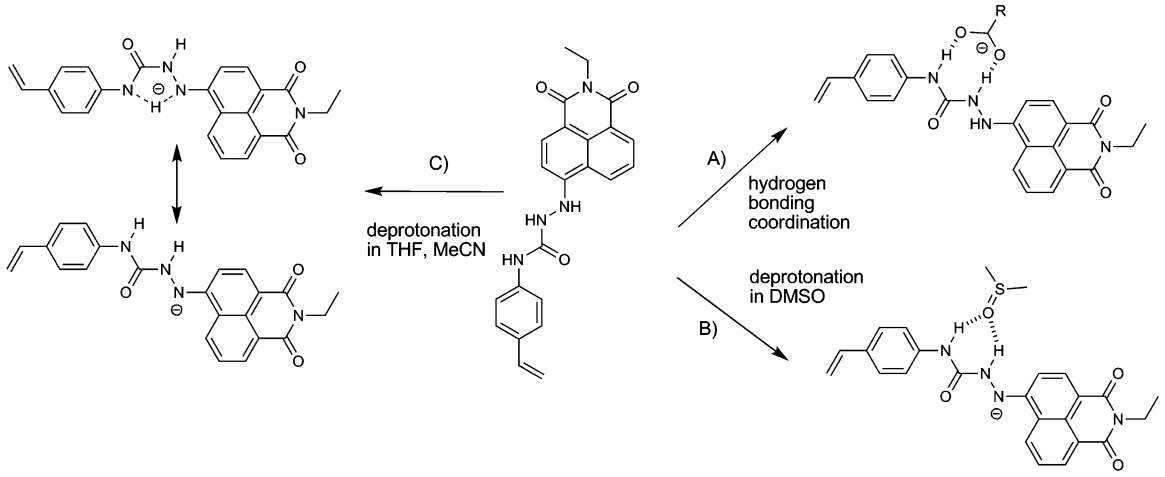

Table 2. Apparent Association Constants K [M^{-1}] for the Interaction between 1 and TBAB in DMSO, MeCN, and THF As Derived from the Spectrophotometric Titration Data in the Range of 1−600 μM TBAB (c_1 = 7 μM) Fitted to a 1:1 Interaction Model at Different Wavelengths; the Latter in (nm) Are Given in Parentheses (r Was Always >0.99)

DMSO	MeCN	THF
	1.1 ± 0.1 × 10^5 (400)	1.5 ± 0.1 × 10^6 (403)
1.1 ± 0.1 × 10^4 (430)		5.6 ± 0.2 × 10^5 (435)
1.0 ± 0.1 × 10^4 (560)	1.6 ± 0.3 × 10^5 (555)	3.0 ± 0.1 × 10^6 (565)

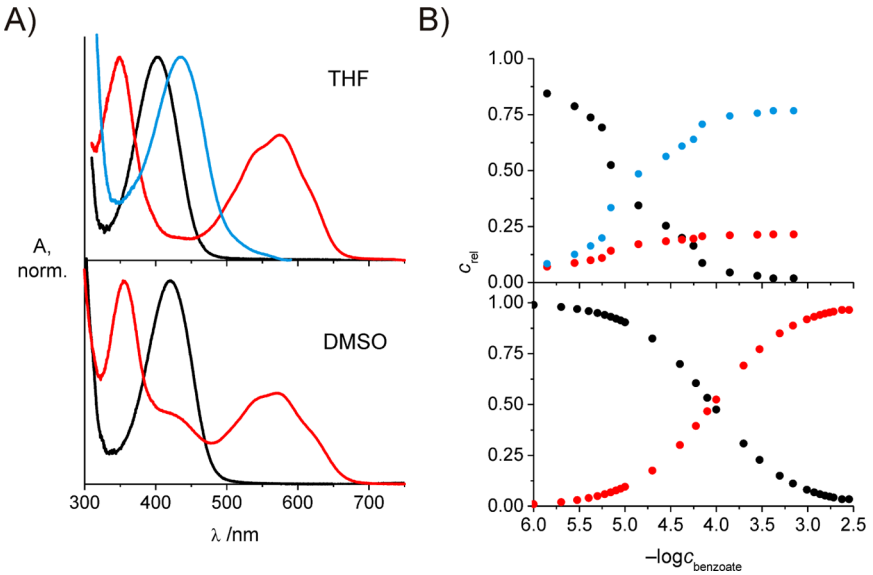

Figure 4. Fitting results for the titrations in THF and DMSO shown in Figure 3. Species spectra (A) and relative concentrations during the course of the titration (B) of **1** (black), $\mathbf{1}^-$ (red), and $\mathbf{1}\subset Bz^-$ (blue) are shown; solvents are indicated.

agreement with the data in Table 2 and the sharp isosbestic points in Figure 3; i.e., they reveal a stoichiometric equilibrium. The corresponding species spectra are shown in Figure 4A, and the development of the relative concentration of species **1** (black) and $\mathbf{1}^-$ (red) is shown in Figure 4B. In the case of THF, a 1:1 model does not lead to an acceptable fit. However, when employing a second global equilibrium MH + B^- ⇌ MHB^- (with MHB^- equaling $\mathbf{1}\subset Bz^-$)[34] the fit converges, yielding a log K = 4.79 ± 0.02 for the formation of the hydrogen bonded complex. When analyzing the species spectra of **1** (black, Figure 4A), $\mathbf{1}^-$ (red), and $\mathbf{1}\subset Bz^-$ (blue) it is apparent that the nature of the blue species has to lie in between those of **1** and $\mathbf{1}^-$ with regard to electron donor properties, i.e., an increased electron richness at the hydrazinecarboxamide moiety should lead to the bathochromic shift to 435 nm.[35] Thus, a complex between **1** and a carboxylate anion is assumed to be responsible for this species. Turning to acetonitrile, a detailed analysis also supports the observations made in Figure 3; i.e., three species **1**, $\mathbf{1}^-$, and $\mathbf{1}\subset Bz^-$ (with a maximum at 411 nm) are involved. As would be expected, complex formation is weaker in MeCN than in THF (log K = 4.26 ± 0.02).

To get better access to this third species, the desirable one from the point of view of the recognition reaction, it is necessary to suppress deprotonation while maintaining hydro-

dx.doi.org/10.1021/jo3019522 | J. Org. Chem. 2013, 78, 1377−1389

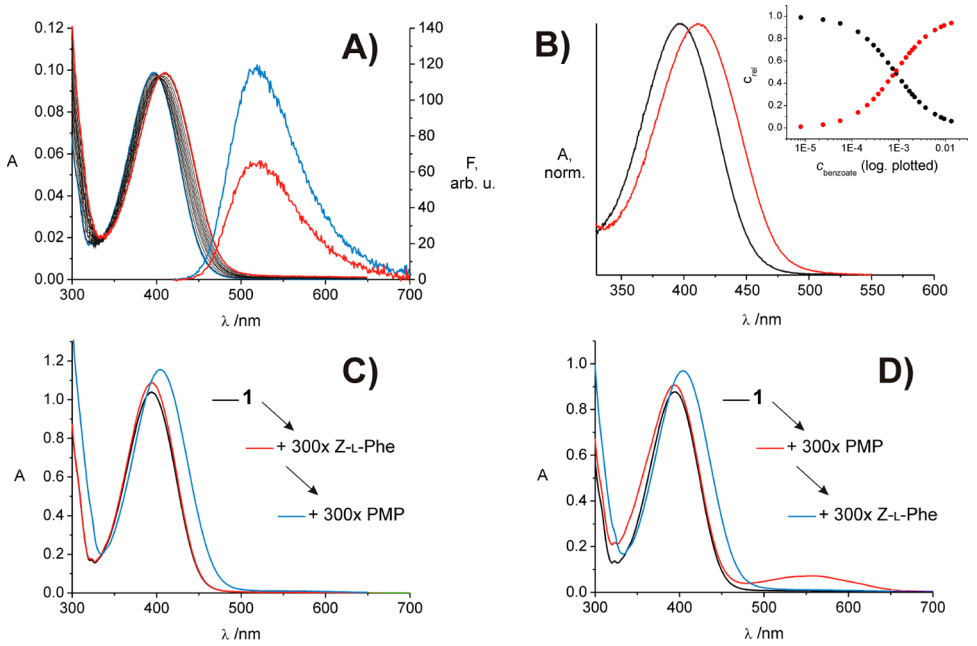

Figure 5. (A) Spectrophotometric titration spectra of **1** (c_1 = 7 μM) upon addition of increasing amounts of a 1:1 mixture of Z-L-Phe and PMP (1−3300 equiv) in MeCN; starting and end point fluorescence spectra are also included. (B) Species spectra of the fitting results (1:1 model) for the corresponding spectrophotometric titration. Spectroscopic changes as a function of addition sequence: **1** followed by an excess Z-L-Phe and the same excess PMP (C) and **1** followed by an excess PMP and the same excess Z-L-Phe (D); excitation in panel (A) at isosbestic point (404 nm).

gen-bond complex formation. We thus turned to a weaker base, Z-L-phenylalanine (Z-L-Phe). Since a carboxylic acid group does not form a complex with a urea binding site, Z-L-Phe has to be turned into the carboxylate in situ. For this purpose, we employed 1,2,2,6,6-pentamethylpiperidine (PMP) in stoichiometric amounts with respect to Z-L-Phe and titrated **1** with this 1:1 mixture of Z-L-Phe and PMP in MeCN (Figure 5A). Apparently, under these conditions and with this analyte, no deprotonation occurs as judged from the virtual absence of the broad band at 570 nm. In addition, the titration shows clear isosbestic points and the development of a new, red-shifted absorption band, which is tentatively ascribed to the hydrogen-bonded complex **1**⊂Z-L-Phe$^-$. Fitting of the titration spectra to a 1:1 binding model reveals two species with maxima of 400 and 412 nm (Figure 5B), the first belonging to the component that is consumed during the titration and the second to the species that is formed (see insert, Figure 5B). We then carried out another set of experiments to confirm these findings. When first an excess of Z-L-Phe is added to **1** in MeCN, the absorption spectrum is virtually unchanged (cf. black and red spectra in Figure 5C). However, when an equal excess of PMP is added, the moderate bathochromic shift is observed (cf. red and blue spectra in Figure 5C). In contrast, when first PMP is added to **1**, a strongly red-shifted band reminiscent of deprotonation is seen (cf. black and red spectra in Figure 5D). Further addition of an excess of Z-L-Phe then reverses the shift and yields the moderately red-shifted band (cf. red and blue spectra in Figure 5D), presumably because of reprotonation of **1** by Z-L-Phe accompanied by complex formation. The complex **1**⊂Z-L-Phe$^-$ thus absorbs at 412 nm in MeCN.

These findings strongly support our assignments made in the TBAB case, i.e., that the band at 435 nm (blue species in Figure 4) belongs to **1**⊂Bz$^-$. The discrepancy between the absolute maxima of the two bands found for **1**⊂Bz$^-$ and **1**⊂Z-L-Phe$^-$, ca. 20 nm, is presumably due to the different electron-donating properties of benzoate and the anion of Z-L-Phe. In addition, the counterion also plays an important role with PMPH$^+$ being able to donate a further directional hydrogen bond but TBA$^+$ being unable to do so, most likely facilitating deprotonation. Plotting and analyzing titration curves of **1** and Z-L-Phe/PMP in MeCN yields log K = 3.08 ± 0.01. Although this value is rather moderate, the combination of **1**/Z-L-Phe/PMP should be suitable for molecular imprinting in polar organic solvents such as acetonitrile.

Fluorescence and NMR Response of 1 toward Carboxylates. Because of their large Stokes shift and considerable brightness, naphthalimide-based probes are well suited for fluorescence assays. If we recall the above-mentioned considerations on the active photophysical processes in such NI dyes and the results shown in Table 1 that the fluorescence quantum yield is reduced with increasing polarity of the solvent, i.e., with an acceleration of the ICT process, the addition of excess electron density to **1**, either through deprotonation or anion binding, is expected to lead to a reduction of the fluorescence of **1** as the exploitable signaling mechanism. Indeed, when the samples shown in Figure 3 are excited into the long-wavelength band at ca. 570 nm, no fluorescence can be recorded. **1**$^-$ is thus virtually nonemissive. In a similar way, the fluorescence spectra shown in Figure 5A suggest that also **1**⊂Z-L-Phe$^-$ is weaker emissive than **1**. The absence of pronounced spectral shifts in emission between **1** and **1**⊂Z-L-Phe$^-$ further suggests that upon excitation the NI-based CT process takes place in the complex, yet that it is less efficient, leading to the reduced fluorescence. The fluorogenic indication mode therefore follows an ON−OFF behavior.

Having established the interaction between **1** and anionic templates by optical spectroscopic means, ^{1}H NMR experiments were conducted in DMSO-d_6 to get further insight into the mechanistic features in the case of benzoate. For the NMR titration, an increasing amount of TBAB was thus added at ratios of 0, 0.25, 0.5, 0.75, 1, 2, 6, 8, and 10 equiv to a constant amount of host monomer. As can be seen from Figure 6, the

dx.doi.org/10.1021/jo3019522 | J. Org. Chem. 2013, 78, 1377−1389

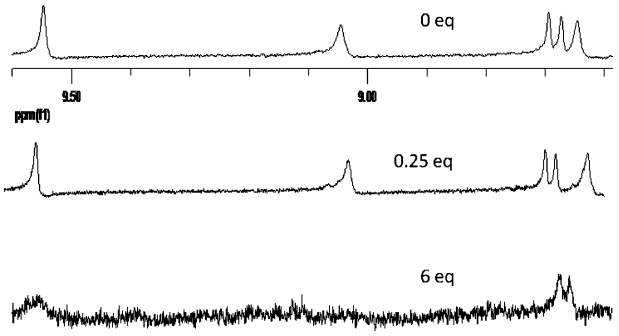

Figure 6. NMR spectra of **1** upon addition of 0, 0.25, and 6 equiv of TBAB in DMSO-d_6.

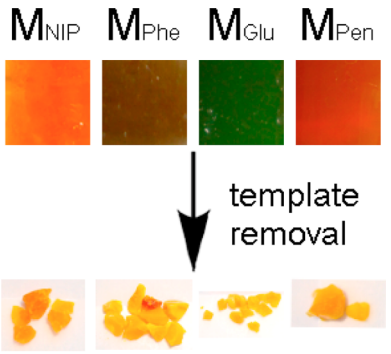

Figure 7. Colors of polymers synthesized from **1** without template (NIP) and in the presence of Z-L-Phe, Z-L-Glu, and PenG prior to and after Soxhlet extraction.

hydrazide proton as well as the urea protons show no complexation induced shift upon addition of increasing amounts of the guest but severe peak broadening accompanied by a decrease in intensity. Apparently, the NMR data support our assumption derived from the UV/vis titrations that the dominant mode of interaction between the fluorescent monomer and benzoate is deprotonation.

Molecularly Imprinted Polymers (MIPs) Prepared from 1. The most common application of MIPs nowadays is still (chromatographic) separation.[36] To be suitable for such purposes, bulk polymers are usually prepared and are subsequently grounded into small (micrometer-sized) particles which are packed into columns. On the other hand, for sensory applications especially with optical interrogation, MIPs are best used in thin-film or (de novo-synthesized) nanoparticle formats.[37,38] To assess the performance of **1** in both formats, we synthesized intrinsically fluorescent monolithic and thin-film MIPs containing **1** and investigated their analyte recognition and discrimination features.

Monolithic Polymers via Bulk Polymerization. Bulk polymers were prepared following the noncovalent stoichiometric approach[39] using a 1:1 ratio between monomer **1** and the respective template. The polymers were formed by free-radical solution polymerization via thermal instead of UV initiation to avoid photobleaching of the dye monomer in the presence of an excess of the cross-linker EDMA (ethylene glycol dimethacrylate). Taking into account the insight gained from the molecular solution studies of **1**, three weakly basic molecules were chosen to serve as templates in the bulk synthesis, namely Z-L-glutamic acid (Z-L-Glu), Z-L-Phe, and penicillin G (PenG). Whereas the amino acids were deprotonated in situ employing PMP, PenG was used as its procain salt. Further details are given in the Experimental Section.

Figure 7 shows that monolithic MIPs could successfully be prepared using **1** as the urea-expressing recognition moiety. Moreover, a comparison of the color of the polymers prepared in the absence (monolithic NIP, termed $\mathbf{M_{NIP}}$ in the following) and in the presence of a template (monolithic MIPs, termed $\mathbf{M_{Phe}}$, $\mathbf{M_{Glu}}$ and $\mathbf{M_{Pen}}$) reveals distinct color differences depending on the template employed. Whereas both $\mathbf{M_{NIP}}$ and $\mathbf{M_{Pen}}$ show a bright orange color prior to and after Soxhlet extraction, the polymer imprinted with Z-L-Phe is brownish and the Z-L-Glu polymer is green. The orange color of $\mathbf{M_{NIP}}$ signifies the reference point of **1** incorporated into an organic polymer matrix. Hence, the only slightly deeper color of $\mathbf{M_{Pen}}$ suggests that this template is primarily incorporated as a hydrogen-bonded complex with **1**. Reconsidering the color changes shown in Figure 2, the much darker colors of $\mathbf{M_{Phe}}$ and $\mathbf{M_{Glu}}$ point to a significant degree of deprotonation; i.e., although used in stoichiometric amounts, Z-L-Glu and Z-L-Phe apparently generated significant amounts of $\mathbf{1}^-$ sites in the monoliths. The orange color after Soxhlet extraction then indicates that all the templates were successfully removed from the polymers and **1** is retained in its neutral form.

Chromatographic Evaluation of Monoliths. After appropriate pretreatment as detailed in the Experimental Section, the crushed polymers (particle size of 25−50 μm) were chromatographically investigated by HPLC analysis employing mobile phases with increasing water content and in the presence and absence of a base modifier. To determine the success of the imprinting step and the cross-selectivity of the polymers, solutions of the respective template and structurally related cross-analytes were injected resulting in the retention results shown in Table 3.

Results for M_{Glu} Columns. Showing a retention time of 5.38 min for the L-enantiomer of Z-Glu and 4.37 min for the D-enantiomer, $\mathbf{M_{Glu}}$ is clearly able to discriminate between its template and the D-enantiomer as well as Z-L-Phe in MeCN/H_2O (50:50); for retention factors k, see Table 3. In contrast, $\mathbf{M_{NIP}}$ shows no retention of both enantiomers. Also in pure MeCN, the retention of the template is stronger for the MIP than for the NIP with a chromatographic imprinting factor $IF_C = k_{ZLGlu}(\mathbf{M_{Glu}})/k_{ZLGlu}(\mathbf{M_{NIP}})$ of 3.32. However, the MIP is not able to discriminate between its template and the cross-analytes Z-D-Glu and Z-L-Phe in pure MeCN, although a clearly enhanced retentivity of Z-Glu on the MIP compared to the NIP was observed. The separation factor for Z-L-Glu, $a_{Glu} = k_{ZLGlu}(\mathbf{M_{Glu}})/k_{ZDGlu}(\mathbf{M_{Glu}})$, equals 1.14. Upon base modification of MeCN with 1% triethylamine (TEA), the retention times are shortened and a worse imprinting factor $IF_C = 1.11$ is obtained. Based on the results discussed above for molecular **1**, we assume that the proneness of the secondary amine function of **1** to deprotonation is enhanced under basic conditions, rendering the designated hydrogen bond-mediated discrimination process less efficient. This contrasts with the "expected" enhanced retentivity observed in presence of basic modifiers for Z-Glu-imprinted polymers prepared using a less acidic urea monomer.[40] In the mobile phase with a high water content of 90% no retention was observed.

Results for M_{Phe} Columns. Different than $\mathbf{M_{Glu}}$, $\mathbf{M_{Phe}}$ shows no enantioselective discrimination in a water-containing mobile phase with a_{Phe} = 1.06 and 0.99 in MeCN/H_2O (10:90) and (50:50) (Table 3). The imprinting factor is small in MeCN/

dx.doi.org/10.1021/jo3019522 | J. Org. Chem. 2013, 78, 1377−1389

Table 3. Chromatographic Performance of M_{Glu}, M_{Phe}, and M_{Pen} in Selected Solvents upon Injection of the Analytes Investigated Here

mPh[a]	pol[b]	k_{ZLGlu}[c]	k_{ZDGlu}	a_{Glu}[d]	k_{ZLPhe}	k_{ZDPhe}	a_{Pheu}	k_{PenG}	k_{BA}
MeCN/H_2O 10:90	M_{Glu}	0.00	0.00		0.00				
	M_{Phe}	0.00			1.44	1.36	1.06		
	M_{Pen}							100.00	0.00
MeCN/H_2O 50:50	M_{Glu}	5.23	4.06	1.29	1.30				
	M_{Phe}	0.42			1.00	1.01	0.99		
	M_{Pen}							100.00	0.00
MeCN	M_{Glu}	2.66	2.33	1.14	2.25				
	M_{Phe}	0.00			7.78	0.55	14.15		
	M_{Pen}								
MeCN (1% TEA)	M_{Glu}	0.60	0.59	1.02	0.27				
	M_{Phe}	0.00			1.92	1.92	1.00		
	M_{Pen}							0.00	0.00

[a]Mobile phase. [b]Polymer. [c]Retention factor $k = (t_{analyte} - t_{void\ marker})/t_{void\ marker}$ with t = retention time [min] and acetone injected as void marker. [d]Separation factor, see text.

H_2O (10:90), yet again substantial in MeCN/H_2O (50:50) with IF_C = 14.3. Again, the retention time for the template Z-L-Phe is significantly higher than for the D-enantiomer in MeCN (a_{Phe} = 14.1), and a high IF_C = 9.85 is also obtained for Z-L-Phe. Like for M_{Glu}, addition of base also leads to a diminution of the imprinting factor (IF_C = 2.02) here, and the enantioselectivity is lost. It is assumed that the significantly higher retention of the template in the Z-L-Phe case is due to enhanced side chain stiffness or aromatic interactions between the template and the monomer.

Results for M_{Pen} Columns. For solubility reasons, PenG was injected as either its procain or potassium salt. The template is fully retained using mobile phases with water content, whereas benzoic acid used as a control is not retained. As in the case of the Z-Phe-imprinted polymer a strong imprinting effect was observed in MeCN–water mixtures, whereas in MeCN and the base-modified MeCN both analytes are eluting fast.

Collectively, the above results demonstrate successful imprinting for all templates with particularly strong imprinting effects seen using MeCN as the mobile phase and Z-Phe and PenG as templates.

Spectroscopic Studies of Monoliths. As can be seen in Figure 7, the monoliths as such are very deeply colored and do not qualify for spectroscopic studies. They are not transparent, precluding conventional absorption and fluorescence measurements in transmission modes. Moreover, if one would use reflectance or front-face setups, only the spectroscopic features of the first nano- or micrometers could be assessed and not the features of the entire bulk. The monoliths thus had to be used in grounded form by suspending 10 mg of polymer in a 96-well plate prior to the analytical measurements in a fluorescence plate reader. First, the free accessibility of **1** in the polymer network was confirmed by recording the fluorescence spectra in solvents of different polarity, revealing also a positive solvatochromism as found for **1** before (Table 4).

Spectroscopic studies of the polymers in the presence of their templates revealed that a change in the emission intensity is only induced in water. To quantify the performance in fluorescence mode, we calculated a (fluorescence) quenching imprinting factor IF_Q by dividing the reduced fluorescence signal $(F_0 - F_\infty)/F_0$ obtained for a MIP at the saturation concentration (plateau at the end of a titration) of a particular analyte by the corresponding reduced fluorescence signal of the NIP (eq 1). If the analyte is bound better in the MIP,

Table 4. Position of Maximum Emission Wavelength of M_{NIP}, M_{Glu}, M_{Phe}, and M_{Pen} in Selected Solvents

	λ_{em} /nm			
solvent	M_{NIP}	M_{Glu}	M_{Phe}	M_{Pen}
dioxane	502	498	500	500
THF	508	500	502	506
MeCN	510	508	510	508
EtOH	514	510	514	516

quenching should be more efficient and as F_∞ becomes smaller $(F_0 - F_\infty)/F_0$ becomes larger; $IF_Q > 1$ are to be expected. For example, M_{Glu} (vs M_{NIP}) shows an IF_Q = 1.4.

$$IF_Q = \frac{\left(\frac{F_0 - F_\infty}{F_0}\right)^{MIP}}{\left(\frac{F_0 - F_\infty}{F_0}\right)^{NIP}} \quad (1)$$

Here, F_0 = fluorescence intensity in the absence of analyte and F_∞ = fluorescence intensity in the presence of analyte at saturation (concentration $c \rightarrow \infty$) of (superscript) MIP or NIP.

No quenching was observed upon addition of only PMP. Thus, the quenching is not a mere deprotonation phenomenon. Nevertheless, none of the grounded monoliths showed discrimination against the cross-analytes employed, for example, Z-D-Glu, Z-L-Phe and PenG for M_{Glu}. Investigation of the swelling behavior in five different solvents, MeCN, MeCN/H_2O (10:90), MeCN/H_2O (50:50), MeCN/TEA (99:1), and water, shows that the swelling in water is not significantly different from that in the other solvent systems to explain the different quenching behavior. The same behavior was also observed for M_{Phe} and M_{Pen}. At present, the peculiar spectroscopic responses of the M_X MIPs are not entirely clear. However, it has to be noted that the dye concentration is rather high in the bulks so that dye–dye interactions such as reabsorption and self-quenching phenomena, which can differ in different solvents, cannot be ruled out.

Thin-Film Polymers on Glass Coverslips. For optical-sensing applications, thin transparent polymer films covalently anchored to glass substrates are an ideal format to handle such responsive layers in actual devices. On the basis of the results obtained with the monolithic polymers (cf. Figure 7), it is essential to have a straightforward and defined optical response, i.e., to use sufficiently low dye concentrations and to avoid as

dx.doi.org/10.1021/jo3019522 | J. Org. Chem. 2013, 78, 1377–1389

much any undesired deprotonation reactions during the polymerization of the sensory MIP. Although the analyte might be retained in a polymer containing certain degrees of deprotonated dye monomer, like the behavior of the deeply colored $\mathbf{M}_{Glu}$ and $\mathbf{M}_{Phe}$ discussed above suggests, all $\mathbf{1}^-$ sites would not be available for the desired indication reaction (hydrogen bond complex formation between **1** and carboxylate) in a sensory MIP. The quest was thus to find a solvent for the MIP preparation that maintains a high degree of hydrogen-bonded complex between **1** and template, that is suitable for the synthetic steps as such, and that yields transparent polymer films. Because the equilibria between complex formation and deprotonation depend not only on solvent/porogen but also on species concentration and the nature of additional reaction partners (comonomer, cross-linker), it was necessary to spectroscopically study the prepolymerization mixtures and assess the degree of deprotonation of **1** to be actually expected in the reaction mixture.

After various attempts, toluene crystallized as the best suitable solvent for our purposes. The absorption maximum of **1** dissolved in toluene is centered at 384 nm (Figure 8, red

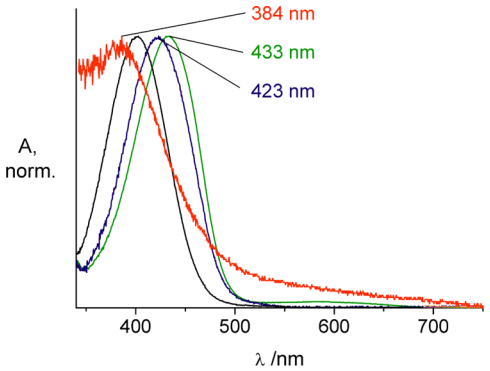

Figure 8. Absorption spectra of prepolymerization mixtures of **1**⊂Z-L-Phe in toluene/MMA/EDMA (blue) and HEMA/EDMA (black); reference points are **1**⊂Z-L-Phe in toluene (green) and **1** in toluene (red).

curve), still hypsochromically shifted compared with the slightly more polar 1,4-dioxane (Table 1). The successful complex formation with Z-L-Phe is then evident from the shift of the absorption band to 433 nm (Figure 8, green curve). Furthermore, upon addition of the other reaction partners MMA and EDMA at their respective concentrations, a shift from 433 to 423 nm is induced (Figure 8, blue curve), indicating a slight weakening of the hydrogen bonded complex by the presence of these compounds of higher polarity. Nevertheless, the complex should be sufficiently stable for film formation and, what is even more important, the virtual absence of the band at ca. 570 nm suggests that deprotonation of **1** is completely avoided especially in the final reaction mixture. A HEMA/EDMA mixture on the other hand leads to significant dissociation of the complex (Figure 8, black curve, maximum at 402 nm) and was discarded here. Thus, thin-film polymers were prepared on glass coverslips in toluene using TBA Z-L-Phe as template, MMA as comonomer and EDMA as cross-linker. Subsequent evaluation was carried out in MeCN. In the present approach, MMA and EDMA were used at ratios that correspond to a cross-linking level of 25%, which is high enough to endow the films with sufficient stability for reuse and which yields promising sensing results, vide infra. In order to assess the reusability of the films and the robustness of the preparation procedure the films were repeatedly extracted and reused. Furthermore, the obtained results were compared to the ones of a second batch of films yielding deviations lower than 5% in all cases.

Spectroscopic investigation of the films in different solvents revealed that the position of the emission maximum is distinctly bathochromically shifted with respect to the values obtained for **1** molecularly dissolved in solution (compare Tables 5 and 1).

Table 5. Position of Maximum Emission Wavelength of $F^{M/E}_{NIP}$, $F^{M/E}_{Phe}$, $F^{B/E}_{NIP}$, and $F^{B/E}_{Phe}$ in Selected Solvents

	λ_{em} /nm			
solvent	$F^{M/E}_{NIP}$	$F^{M/E}_{Phe}$	$F^{B/E}_{NIP}$	$F^{B/E}_{Phe}$
dioxane	466	467	465	465
THF	470	471	472	471
MeCN	480	480	481	480
EtOH	480	480	481	481

Apparently, when the dye monomer is integrated into the polymer full relaxation of the excited state of **1** is precluded by a confinement in the polymer matrix or by a reduced local polarity of the microenvironment. Nevertheless, the films exhibit positive solvatochromism like the free dye monomer in solution; the sites should thus be well-accessible. Sensing tests with imprinted Z-L-Phe as analyte in acetonitrile in a custom-build quartz cuvette (measured with a fluorometer in front-face mode) revealed a positive response, that is, the fluorescence of the $F^{M/E}_{Phe}$ MIPs was significantly stronger quenched than that of the corresponding NIPs, $F^{M/E}_{NIP}$; terminology: $F^{M/E}_{Phe}$ = ***F***ilms prepared with ***M***MA/***E***DMA (superscript) as comonomer and cross-linker and Z-L-***Phe*** (subscript) as template. A clear imprinting effect was observed (Figure 9). However, because

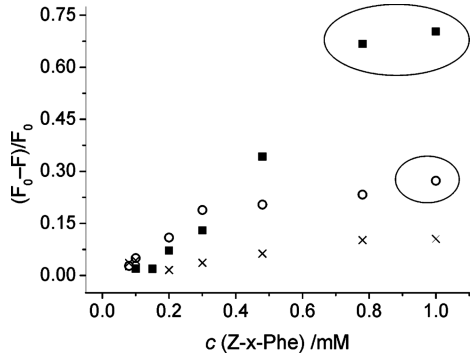

Figure 9. Titration curves of $F^{M/E}_{Phe}$ in the presence of Z-L-Phe (squares) and Z-D-Phe (circles) as well as $F^{M/E}_{NIP}$ in the presence of Z-L-Phe (crosses) in acetonitrile; encircled data points at higher concentrations belong to spectra that show already contributions of deprotonation; i.e., the quenching recorded for these points is disproportionally large.

the spectra at concentrations above 0.5 mM indicated deprotonation side reactions, IF_Q = 3.4 was determined at c = 0.5 mM from Figure 9. Since a clear onset of fluorescence quenching was recorded only for c = 0.1 mM, the dynamic working range is rather limited (Figure 9). The next step was to investigate the enantioselectivity of the MMA/EDMA films. For this purpose, the fluorescence signals observed for Z-L-Phe-imprinted $F^{M/E}_{Phe}$ upon addition of Z-L-Phe and Z-D-Phe were analyzed according to eq 2, arriving at the discrimination factor

dx.doi.org/10.1021/jo3019522 | J. Org. Chem. 2013, 78, 1377−1389

derived from fluorescence quenching q (which corresponds phenomenologically to a of the HPLC section).

$$q = \frac{\left(\frac{F_0 - F_\infty}{F_0}\right)^{\mathrm{LMIP}}_{\mathrm{L}}}{\left(\frac{F_0 - F_\infty}{F_0}\right)^{\mathrm{LMIP}}_{\mathrm{D}}} \quad (2)$$

Here, F_0 = fluorescence intensity of (superscript) L-enantiomer-imprinted MIP in the absence of analyte and F_∞ = fluorescence intensity in the presence of analyte (L- or D-enantiomer, subscripts L and D) at saturation (concentration $c \rightarrow \infty$). For $F^{M/E}_{Phe}$ in MeCN, this discrimination factor is obtained to q_{Phe} = 1.7 (again at c = 0.5 mM) for Z-L-Phe vs Z-D-Phe, suggesting favorable enantioselectivity (Figure 9).

Exchange of MMA for BMA. Taking into account that Z-L-Phe contains an aromatic moiety, the system was fine-tuned by substituting the aliphatic comonomer MMA with an aromatic one, benzyl methacrylate (BMA). We assumed that the affinity of the aromatic template toward the polymer should be enhanced by additional $\pi\pi$ interactions. As displayed above for the MMA/EDMA films the emission bands of the BMA/EDMA films are also shifted to shorter wavelengths with respect to molecularly dissolved **1** (Table 5).

The response of the films toward their template and the cross-selectivity to structurally closely related compounds was investigated in pure MeCN, mixtures with increasing water content, and a base-modified system. In MeCN, the MIP films showed remarkable quenching upon addition of the template, and a clear imprinting effect of IF_Q = 18.6 was obtained (Figure 10). Similar results were found in MeCN/TEA (99:1). To

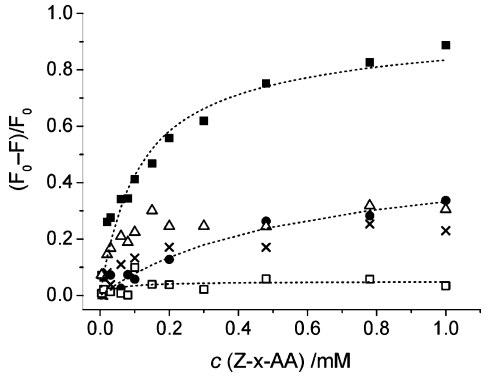

Figure 10. Titration curves of $F^{B/E}_{Phe}$ in the presence of Z-L-Phe (solid squares), Z-D-Phe (circles), Z-L-Glu (crosses), and Z-L-Tyr (triangles) as well as $F^{B/E}_{NIP}$ in the presence of Z-D-Phe (open squares) in acetonitrile; lines are only guides to the eye for $F^{B/E}_{Phe}$ /Z-L-Phe, $F^{B/E}_{Phe}$ /Z-D-Phe and $F^{B/E}_{NIP}$ /Z-D-Phe; AA = amino acid.

assess the performance against the other enantiomer and closely related analytes, the response of $F^{B/E}_{Phe}$ and $F^{B/E}_{NIP}$ toward TBA Z-D-Phe, TBA Z-L-Glu, being aliphatic in nature yet carrying two carboxylate groups, and TBA Z-L-Tyr as an aromatic competitor was investigated. The enantioselective discrimination with q_{Phe} = 2.8 was found to be better than in the case of $F^{M/E}_{Phe}$. Even more pronounced was the discrimination obtained against the structural analogues, i.e., $q_{Phe/Glu}$ of 4.7 and $q_{Phe/Tyr}$ of 3.3 were found against Z-L-Glu and Z-L-Tyr. As could be expected, the difference is more pronounced in the case of the aliphatic amino acid (Figure 10).

To assess the influence of base addition and the possibility to further increase the discrimination ability, the studies were repeated in the base-modified solvent mixture. Again, fluorescence quenching was observed, arriving at q = 1.2, 1.6, and 1.3 for Z-L-Phe against Z-D-Phe, Z-L-Glu, and Z-L-Tyr, which are not as high as in the neat polar solvent, reflecting the behavior observed in the monoliths above. Most likely deprotonation plays also a role in this case. Detailed analyses however were precluded by the low optical density of the thin films which made reliable quantitative absorption measurements impossible.

BMA/EDMA MIP Films against Penicillin G Potassium Salt. In a final attempt to assess the first performance criteria of intrinsically fluorescent MIP thin films, penicillin G potassium salt was imprinted according to the same recipe as used before in the films for amino acids. The spectroscopic features were again evaluated in MeCN, base-modified MeCN and mixtures with increasing water content. However, different from the monoliths, fluorescence quenching in the presence of PenG could only be observed in MeCN, arriving at an IF_Q of 2.5 (Figure 11).

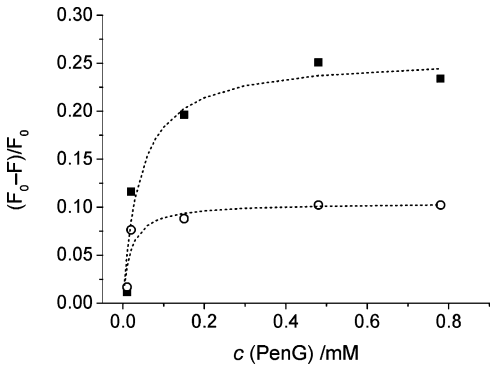

Figure 11. Titration curves of $F^{B/E}_{Phe}$ (squares) and $F^{B/E}_{NIP}$ (circles) in the presence of PenG in acetonitrile; the lines are only guides to the eye.

CONCLUSION

A novel polymerizable naphthalimide monomer was designed and synthesized, incorporating a urea binding site and showing the favorable spectral features of naphthalimide chromophores such as broad and strongly Stokes' shifted absorption and emission bands in the visible spectrum. Detailed investigations of the title compounds and several other model NI dyes allowed us to unravel the quenching mechanisms in *N*-nitrogen substituted 4-amino-NIs. Being rather acidic in nature, titrations of **1** with TBA benzoate in various solvents and a comprehensive analysis of the titration spectra provided deeper insight into the dualism between deprotonation and complex formation. Whereas the fluorescent monomer is not able to bind rather strong bases like benzoate only in the designated fashion, the formation of a directionally oriented hydrogen-bonded complex should yield much better imprinting results than the nondirectional purely electrostatic association of ionic species, the experiments employing Z-L-Phe yielded very promising results in terms of the imprinting of such weakly basic carboxylates. Accordingly, MIP synthesis was attempted and title compound **1** could be successfully integrated in polymers of monolithic and thin-film format. Upon chromatographic evaluation, the bulk polymers showed remarkable recognition behavior; enantioselective discrimination was

dx.doi.org/10.1021/jo3019522 | J. Org. Chem. 2013, 78, 1377−1389

obtained. However, spectroscopic studies of the crushed monoliths (as microparticles) revealed that these polymers are not suitable for sensing applications, leaving the spectroscopic features of the materials rather unchanged in presence of oxyanionic analytes.

The step to thin-film polymers covalently attached to glass supports composed of monomer **1**, MMA or BMA, respectively, and EDMA then allowed to obtain sensory MIPs with a rather low cross-linking level of 25% yet with sufficient stability of the films for reuse in analytical experiments. Investigation of the spectroscopic and analyte-responsive behavior of the films revealed that in all cases the imprinting step was successful with the polymers being able to chirally discriminate between their respective template and structurally closely related cross-analytes especially when employing the aromatic comonomer. Finally summarizing the observations made during the present studies of the various MIP formats, i.e., good enantioselective separation but weak sensing responses for monolithic MIPs which contain a considerable degree of deprotonated dye monomer (see for instance the deep colors of some of the monoliths in Figure 7) and a good sensing behavior yet lower discrimination ability (e.g., $q_{Phe} = 2.8$ for $F^{B/E}_{Phe}$ in MeCN vs $a_{Phe} = 14.15$ for $\mathbf{M_{Phe}}$ in MeCN) for the thin-film MIPs with intact (protonated) functional urea monomers it seems obvious that a lot of the cavities formed in the bulks retain the template without the directional hydrogen-bonding participation of the designated urea host monomer. These deprotonated ureas will mainly interact through nondirectional electrostatic forces, i.e., the ureas contribute to template binding during the polymerization process yet the cavity formed might preclude the spectroscopically desired H bond complex formation during the rebinding step. These rebound molecules will remain spectroscopically silent and the desired fluorescence quenching response is triggered only from that fraction of cavities which can and will accommodate the template in the desired fashion through H-bonding. On the other hand, the cavities in the thin-film MIPs are not only able to discriminate between different analytes, but also show enantioselective discrimination. Further research in our laboratories primarily addresses the detailed unraveling of the specific vs unspecific and designated vs bulk recognition and the improvement of the 3D rigidity of the thin-film MIPs.

EXPERIMENTAL SECTION

***N*-Ethyl-4-hydrazino-1,8-naphthalimide (3).** Compound **2** (120 mg, 0.39 mmol) was dissolved in 30 mL of 1,4-dioxane. Hydrazine monohydrate (2.5 mL) was added dropwise. The solution was stirred at 60 °C for 18 h. After being cooled to room temperature, the reaction mixture was poured into water. The precipitated solid was collected by filtration, washed with water, and dried, yielding a yellow solid. Yield = 90 mg (0.35 mmol, 90%). ^{1}H NMR (300 MHz, DMSO-d_6) δ: 1.14 (t, 3H), 4.01 (q, 2H), 4.63 (s, 2H), 7.20 (d, 1H), 7.58 (dd, 1H), 8.24 (d, 1H), 8.37 (d, 1H), 8.56 (dd, 1H), 9.07 (s, 1H). MS, *m*/*z*: found 256.10 g mol^{-1} [M + H]$^+$, calcd mass 255.10 g mol^{-1}.

1-Isocyanato-4-vinylbenzene. Following a modified procedure of ref 41 in a first step, *p*-bromomethylbenzoic acid (11.50 g, 54 mmol) and triphenylphosphine (14.10 g, 54 mmol) were dissolved in 250 mL of acetone and refluxed for 3 h. The warm mixture was precipitated from 1 L of diethyl ether. The precipitated salt was filtered off and dried under vacuum. Yield: 97%. ^{1}H NMR (300 MHz, DMSO-d_6) δ: 5.26 (d, 2H, J = 12 Hz), 7.09 (q, 2H), 7.74 (m, 14H), 7.92 (m, 3H), 13.11 (s, 1H). MS, *m*/*z*: found 397.14 g mol^{-1} [M − Br]$^-$, calcd mass 397.14 g mol^{-1}. Next, (4-carboxyphenyl)-methyltriphenylphosphonium bromide (24.6 g, 50 mmol) was dissolved in 100 mL of formaldehyde in water (37%). The solution was cooled to 0 °C, and 100 mL 0.5 M NaOH was added dropwise. The mixture was stirred 48 h at room temperature. The solid was removed by filtration and washed with 1 M NaOH solution. The filtrate was acidified with 10% HCl solution to precipitate the product. The product was dried and recrystallized from ethanol/water 3:7. Yield: 89%. ^{1}H NMR (300 MHz, DMSO-d_6) δ: 5.37 (d, 1H, J = 9 Hz), 5.94 (d, 1H, J = 12 Hz), 6.80 (dd, 1H, J = 12 Hz, 9 Hz), 7.54 (d, 2H, J = 6 Hz), 7.89 (d, 2H, J = 6 Hz), 8.39 (s, 1H). ^{13}C NMR (DMSO-d_6) δ: 117.9, 127.1, 130.5, 130.8, 136.7, 142.1, 167.9. MS, *m*/*z*: found mass 148.55 g mol^{-1}, calcd mass 148.16 g mol^{-1}. For the subsequent transformation of 4-vinylbenzoic acid into 1-isocyanato-4-vinylbenzene, ethyl chloroformate as the chlorination agent and NaN_3 were used in accordance with a protocol published in ref 42.Yield: 62%. ^{1}H NMR ($CDCl_3$) δ: 5.24 (dd, 1H), 5.71 (dd, 1H), 6.65 (dd, 2H), 7.02 (d, 2H), 7.34 (d, 2H); MS, *m*/*z*: found mass 145.10 g mol^{-1}, calcd mass 145.01 g mol^{-1}.

***N*-Ethyl-4-(*N*-[4-vinylphenyl]hydrazinecarboxamidyl)-1,8-naphthalimide (1).** The reaction was carried out under inert gas atmosphere. Compound **3** (150 mg, 0.59 mmol) was dissolved in 12 mL of THF/pyridine (50:50, v/v). 1-Isocyanato-4-vinylbenzene (85 mg, 0.59 mmol) in 12 mL of THF/pyridine (50:50, v/v) was added dropwise. The solution was stirred at 28 °C for two days under nitrogen atmosphere, precipitated from *n*-hexane, filtrated, and dried, yielding a yellow solid. Yield = 136.88 mg (0.34 mmol, 58%). Mp: 245−247 °C. ^{1}H NMR (400 MHz, DMSO-d_6) δ: 1.15 (t, J = 7.0 Hz, 3H), 4.03 (q, J = 7.0 Hz, 2H), 5.08 (d, J = 11.7 Hz, 1H), 5.64 (d, J = 17.6 Hz, 1H), 6.60 (dd, J = 17.7, 10.8 Hz, 1H), 7.01 (d, J = 8.5 Hz, 1H), 7.39 (q, J = 29.6, 8.5 Hz, 4H), 7.73 (m, 1H), 8.33 (d, J = 8.4 Hz, 1H), 8.46 (d, J = 6.7 Hz, 1H), 8.64 (s, 1H), 8.68 (d, J = 8.6 Hz, 1H), 9.04 (s, 1H), 9.55 (s, 1H). ^{13}C NMR (500 MHz, DMSO-d_6) δ: 13.3, 34.2, 103.9, 107.3, 112.0, 118.0, 118.4, 121.7, 124.0, 126.6, 128.2, 129.2, 130.4, 130.8, 134.1, 136.2, 139.3, 152.2, 153.1, 162.6, 163.5. HRMS: calcd for $C_{23}H_{21}O_3N_4$ [M + H]$^+$ 401.1608, found 401.1608.

Tetrabutylammonium Benzoate (TBAB). Benzoic acid (272 mg, 2.2 mmol) was dissolved in 10 mL of dry methanol. A 1 M solution of tetrabutylammonium hydroxide (1 equiv, 2.23 mL) in methanol was added dropwise. The mixture was stirred for 2 h at room temperature. After solvent removal, the product was dried over P_2O_5.

Bulk Polymers. The bulk polymers were prepared according to the ratios displayed in Table S1 (Supporting Information) and the following procedure (with the example of $\mathbf{M_{Glu}}$). Z-L-Glu (0.25 mmol) and PMP (0.5 mmol) were dissolved in anhydrous DMF (5.6 mL). Subsequently, **1** (0.5 mmol) and EDMA (20 mmol) were added. After addition of the azo-initiator ABDV (1% w/w total monomers), the prepolymerization mixture was transferred to a polymerization tube, purged with dry nitrogen, and polymerized at 45 °C for 24 h. The obtained polymers were crushed and extracted by Soxhlet for 24 h with MeOH/HCl (0.5 mM) (80:20 v/v) and 24 h with MeOH. Anal. Calcd for $\mathbf{M_{Glu}}$: C, 61.00; H, 7.02; N, 0.67. Found: C, 60.24; H, 7.51; N, 0.70. Anal. Calcd for $\mathbf{M_{Phe}}$: C, 61.00; H, 7.02; N, 0.67. Found: C, 60.57; H, 7.54; N, 0.75. Anal. Calcd for $\mathbf{M_{Pen}}$: C, 61.00; H, 7.02; N, 0.67. Found: C, 60.43; H, 7.74; N, 0.76. Anal. Calcd for $\mathbf{M_{NIP}}$: C, 61.00; H, 7.02; N, 0.67. Found: C, 60.30; H, 7.43; N, 0.75. All polymers show good agreement between measured and calculated values. Thus, it can be concluded that the polymer synthesis was successful and the monomers were integrated into the polymers quantitatively.

Thin-Film Polymers on Glass Coverslips. Pretreatment. Three hundred coverslips were precleaned for 12 h with concd KOH solution and subsequently carefully rinsed with water. To activate the surface, the coverslips were left in piranha solution overnight, rinsed with water, acetone, and toluene, and dried. The linker 3-methacryloxypropyltrimethoxysilane was immobilized by stirring the coverslips in a solution of the linker (20 mL) and triethylamine (7 mL) in toluene (150 mL). Subsequently, the coverslips were washed with toluene and methyl *tert*-butyl ether (MTBE) and dried.

Polymer-Film formation. Compound **1** (0.06 mg, 0.15 μmol), TBA Z-L-Phe (equimolar to **1**), MMA or BMA, respectively (12.86 μL, 0.11 mmol), and ethylene glycol dimethacrylate (EDMA, 8.58 μL, 0.04

dx.doi.org/10.1021/jo3019522 | J. Org. Chem. 2013, 78, 1377−1389

mmol) were dissolved in 25 μL of toluene. The prepolymerization mixtures were flushed with nitrogen, and the azo-initiator ABDV was added. Subsequently, 2 μL of the solutions was dropped onto a glass slide and covered with a 3-methacryloxypropyltrimethoxysilane-modified coverslip. Polymerization was initiated thermally by heating with a heat-gun three times for 10 s and subsequently in the oven at 70 °C for 1 h. The obtained polymer films were extracted using a Soxhlet apparatus with MeOH. The NIPs were prepared accordingly, without addition of the template. Representative SEM images can be found in the Supporting Information.

Spectroscopic Studies. Reagents. Compund **10** was a gift from Dipl.-Chem. S. Ast and Prof. H.-J. Holdt (University of Potsdam).

Instruments and Methods. Absorption spectra and UV/vis spectrophotometric titrations were recorded on a UV/vis spectrophotometer, and fluorescence spectra and titrations were measured with a spectrofluorometer (molecular dye, thin-film polymers) or a microplate reader (crushed monoliths, in bottom reading mode) at 298 ± 1 K. Unless otherwise noted, only dilute solutions with an absorbance of less than 0.1 at the absorption maximum were used for the molecular studies. The fluorescence quantum yields (Φ_f) were determined relative to coumarin 153 in ethanol ($\Phi_f = 0.544$),[43] respectively. The uncertainties of measurement were determined to ±5% (for $\Phi_f > 0.2$), ±10% (for $0.2 > \Phi_f > 0.02$), and ±20% (for $0.02 > \Phi_f$). Fluorescence lifetimes (τ_f) were determined by a unique customized laser impulse fluorometer with picosecond time resolution.[44,45] Further details on the fluorescence decay time measurements can also be found in ref 45. The uncertainty of measurement amounted to ±3 ps. The fluorescence lifetime profiles were analyzed with a PC using the software package Global Unlimited V2.2 (Laboratory for Fluorescence Dynamics, University of Illinois). The goodness of the fit of the single decays as judged by reduced χ-squared (χ_R^2), and the autocorrelation function $C(j)$ of the residuals was always below $\chi_R^2 < 1.2$.

Data Analysis. Fitting of the titration data to reaction equilibria was done with HypSpec 1.1.39 from Protonic Software (Leeds).

HPLC Evaluation of Bulk Polymers. The monolithic polymers were crushed to a particle size between 25 and 50 μm. To remove smaller particles, this size fraction was repeatedly sedimented (80/20 methanol/Millipore water) and then slurry-packed into stainless-steel HPLC columns (2.5 × 0.4 cm) using the same solvent mixture as pushing solvent. Prior to usage the columns were first washed with methanol to ensure the complete removal of template. Subsequent analysis of the polymers was performed with a HPLC system with a diode array-UV detector. Analyte detection was performed at 205 and 260 nm (Z-Glu, Z-Phe) and 220 nm PenG. To evaluate the polymers ability to discriminate between its template, the other enantiomer and cross-analytes, solutions of Z-L-Glu, Z-D-Glu, and Z-L-Phe were injected. The Glu solutions were prepared in the corresponding mobile phases, concentration of 10 mM, injection volume 10 μL. Because of the poor solubility of Z-L-Phe in mobile phases with high water content, the concentration was lowered to 1 mM, injection volume 100 μL.

Spectroscopic Evaluation of MIPs. Bulks. Twelve × 10 mg of $\mathbf{M}_{NIP}$ and 24 × $\mathbf{M}_{Glu}$ were incubated for 4 h in a 96-well plate with concentrations between 0 and 1 mM solutions of Z-L-Glu/PMP and Z-D-Glu/PMP in water. Subsequently, emission scans were performed (excitation wavelength: 377 nm; emission wavelength: 390 −800 nm). For the cross-linking studies, emission scans of the respective polymers were performed in DMSO in a 96 well plate in presence of TBA benzoate. The theoretical amount of monomer present was calculated from the preparation recipe, Table S2 (Supporting Information). **Thin Films.** The coverslips with the extracted films were mounted in a custom-made quartz cuvette equipped with a Teflon holder. The fluorescence emission of the films was monitored during titrations with increasing concentration of selected analytes between 0 and 1 mM (excitation wavelength: 380 nm, emission wavelength range: 395−550 nm). The obtained results were background corrected.

Swelling Behavior of the Bulk Polymers. A certain amount of the respective grounded polymer was filled in a NMR tube. The height of the polymer in the tube was measured. Subsequently, 1 mL of the respective solvent was added and the polymers well dispersed. After 24 h, the height of the polymer was measured again. The swelling factor was calculated by dividing the height in swollen state by the height in dry state.

■ ASSOCIATED CONTENT

Supporting Information

^{13}C NMR spectrum of **1**, tables with details of polymer synthesis, SEM images of thin film MIPs. This material is available free of charge via the Internet at http://pubs.acs.org.

■ AUTHOR INFORMATION

Corresponding Author

*Tel: +49 30 81041154 (K.R.), +49 231 7554082 (B.S.). Fax: +49 30 81041157 (K.R.), +49 231 7554084 (B.S.). E-mail: (K.R.) knut.rurack@bam.de, (B.S.) b.sellergren@infu.tu-dortmund.de.

Present Address

#Dow Europe GmbH, Bachtobelstrasse 3, CH-8810 Horgen, Switzerland.

Notes

The authors declare no competing financial interest.

■ ACKNOWLEDGMENTS

This work was supported by the DFG (RU 1622/1-1, SE 777/15-1), the Innovationsfonds of BAM/BMWi, and MICINN (ref CTQ2009-14565-C03). We thank Dr. Marco Emgenbroich for synthetic advice, Dipl.-Chem. Sandra Ast and Prof. Hans-Jürgen Holdt (University of Potsdam) for provision of **10**, Dr. Dietmar Pfeifer (Div. 1.3, BAM) for NMR, and Peter Gans (Protonic Software) for support and further refinement of HypSpec.

■ REFERENCES

(1) Chaterji, S.; Kwon, I. K.; Park, K. *Prog. Polym. Sci.* **2007**, *32*, 1083.
(2) Reppy, M. A.; Pindzola, B. A. *Chem. Commun.* **2007**, 4317.
(3) *Molecularly Imprinted Polymers: Man-Made Mimics of Antibodies and Their Application in Analytical Chemistry*; Sellergren, B., Ed.; Elsevier: Oxford, 2000.
(4) Moreno-Bondi, M. C.; Navarro-Villoslada, F.; Benito-Pena, E.; Urraca, J. L. *Curr. Anal. Chem.* **2008**, *4*, 316.
(5) Subrahmanyam, S.; Piletsky, S. A.; Piletska, E. V.; Chen, B. N.; Day, R.; Turner, A. P. F. *Adv. Mater.* **2000**, *12*, 722.
(6) Chow, C. F.; Lam, M. H. W.; Leung, M. K. P. *Anal. Chim. Acta* **2002**, *466*, 17.
(7) Liao, Y.; Wang, W.; Wang, B. H. *Bioorg. Chem.* **1999**, *27*, 463.
(8) Liu, R. Y.; Guan, G. J.; Wang, S. H.; Zhang, Z. P. *Analyst* **2011**, *136*, 184.
(9) Benito Peña, E.; Moreno-Bondi, M. C.; Aparicio, S.; Orellana, G.; Cedefur, J.; Kempe, M. *Anal. Chem.* **2006**, *78*, 2019.
(10) Urraca, J. L.; Moreno-Bondi, M. C.; Orellana, G.; Sellergren, B.; Hall, A. J. *Anal. Chem.* **2007**, *79*, 4915.
(11) Nguyen, T. H.; Ansell, R. J. *Org. Biomol. Chem.* **2009**, *7*, 1211.
(12) Kubo, H.; Yoshioka, N.; Takeuchi, T. *Org. Lett.* **2005**, *7*, 359.
(13) Ng, S. M.; Narayanaswamy, R. *Anal. Bioanal. Chem.* **2006**, *386*, 1235.
(14) Southard, G. E.; Van Houten, K. A.; Ott, E. W.; Murray, G. M. *Anal. Chim. Acta* **2007**, *581*, 202.
(15) Saha, S.; Samanta, A. *J. Phys. Chem. A* **2002**, *106*, 4763.
(16) Qi, Q.; Ha, Y.-Q.; Sun, Y.-M. *Int. J. Quantum Chem.* **2011**, *111*, 2234.
(17) Niu, C. G.; Zeng, G. M.; Chen, L. X.; Shen, G. L.; Yu, R. Q. *Analyst* **2004**, *129*, 20.
(18) Wang, J. B.; Qian, X. H. *Chem. Commun.* **2006**, 109.
(19) Grabchev, I.; Qian, X.; Xiao, Y.; Zhang, R. *New J. Chem.* **2002**, *26*, 920.

(20) Jiang, J. B.; Leng, B.; Xiao, X.; Zhao, P.; Tian, H. *Polymer* **2009**, *50*, 5681.
(21) Gunnlaugsson, T.; Kruger, P. E.; Lee, T. C.; Parkesh, R.; Pfeffer, F. M.; Hussey, G. M. *Tetrahedron Lett.* **2003**, *44*, 6575.
(22) Veale, E. B.; Tocci, G. M.; Pfeffer, F. M.; Kruger, P. E.; Gunnlaugsson, T. *Org. Biomol. Chem.* **2009**, *7*, 3447.
(23) Hall, A. J.; Quaglia, M.; Manesiotis, P.; De Lorenzi, E.; Sellergren, B. *Anal. Chem.* **2006**, *78*, 8362.
(24) Urraca, J. L.; Moreno-Bondi, M. C.; Hall, A. J.; Sellergren, B. *Anal. Chem.* **2007**, *79*, 695.
(25) Gunnlaugsson, T.; Kruger, P. E.; Jensen, P.; Tierney, J.; Ali, H. D. P.; Hussey, G. M. *J. Org. Chem.* **2005**, *70*, 10875.
(26) Gan, J.; Tian, H.; Wang, Z.; Chen, K.; Hill, J.; Lane, P. A.; Rahn, M. D.; Fox, A. M.; Bradley, D. D. C. *J. Organomet. Chem.* **2002**, *645*, 168.
(27) Li, A.-F.; Wang, J.-H.; Wang, F.; Jiang, Y.-B. *Chem. Soc. Rev.* **2010**, *39*, 3729.
(28) Wintgens, V.; Valat, P.; Kossanyi, J.; Biczok, L.; Demeter, A.; Berces, T. *J. Chem. Soc., Faraday Trans.* **1994**, *90*, 411.
(29) Alexiou, M. S.; Tychopoulos, V.; Ghorbanian, S.; Tyman, J. H. P.; Brown, R. G.; Brittain, P. I. *J. Chem. Soc., Perkin Trans. 2* **1990**, 837.
(30) Sawa, M.; Hsu, T.-L.; Itoh, T.; Sugiyama, M.; Hanson, S. R.; Vogt, P. K.; Wong, C.-H. *Proc. Natl. Acad. Sci. U.S.A.* **2006**, *103*, 12371.
(31) Manuscript in preparation.
(32) Boiocchi, M.; Del Boca, L.; Esteban Gómez, D.; Fabbrizzi, L.; Licchelli, M.; Monzani, E. *J. Am. Chem. Soc.* **2004**, *126*, 16507.
(33) Leng, B.; Tian, H. *Aust. J. Chem.* **2010**, *63*, 169.
(34) The program employed only allows the fitting of microscopic association equilibria of A + B ⇌ AB-type, i.e., M^- + H^+ ⇌ MH, B^- + H^+ ⇌ BH, MH + B^- ⇌ MHB, etc. The spectrum of **1** in DMSO and THF (black species in Figure 4A) and the spectrum of $\mathbf{1}^-$ in THF (red species; obtained by deprotonation of **1** with the spectroscopically silent TBA hydroxide) were included as known species in the fits. Without including $\mathbf{1}^-$ or M as known component in the THF case, convergence of the fit to chemically meaningful result was much more difficult.
(35) The shape of the absorption spectra of $\mathbf{1}^-$ varies somewhat between DMSO and THF which is tentatively ascribed to the various possible isomers/tautomers of $\mathbf{1}^-$ (see also Scheme 2).
(36) Sellergren, B.; Martin Esteban, A., In: *Handbook of Sample Preparation*; Pawlitszyn, J., Lord, H. L., Eds.; John Wiley & Sons Inc.: NJ, 2010, pp 445−475.
(37) Mayes, A. G.; Whitcombe, M. J. *Adv. Drug Delivery Rev.* **2005**, *57*, 1742.
(38) Tokonami, S.; Shiigi, H.; Nagaoka, T. *Anal. Chim. Acta* **2009**, *641*, 7.
(39) Andersson, L.; Sellergren, B.; Mosbach, K. *Tetrahedron Lett.* **1984**, *25*, 5211.
(40) Hall, A. J.; Manesiotis, P.; Emgenbroich, M.; Quaglia, M.; De Lorenzi, E.; Sellergren, B. *J. Org. Chem.* **2005**, *70*, 1732.
(41) Porcal, W.; Hernández, P.; Aguirre, G.; Boiani, L.; Boiani, M.; Merlino, A.; Ferreira, A.; Di Maio, R.; Castro, A.; González, M.; Cerecetto, H. *Bioorg. Med. Chem.* **2007**, *15*, 2768.
(42) Luebke, M.; Whitcombe, M. J.; Vulfson, E. N. *J. Am. Chem. Soc.* **1998**, *120*, 13342.
(43) Rurack, K.; Spieles, M. *Anal. Chem.* **2011**, *83*, 1232.
(44) Resch, U.; Rurack, K. *Proc. SPIE-Int. Soc. Opt. Eng.* **1997**, *3105*, 96.
(45) Shen, Z.; Röhr, H.; Rurack, K.; Uno, H.; Spieles, M.; Schulz, B.; Reck, G.; Ono, N. *Chem.—Eur. J.* **2004**, *10*, 4853.